Journal of Engineering Science and Technology
Vol. 14, No. 4 (2019) 2271 - 2291

EFFECTS OF PROCESS PARAMETERS AND ALLOYING ELEMENTS ON MICRO-HARDNESS DISTRIBUTION IN PULSE ARC 304L AUSTENITIC STAINLESS STEEL WELDED PLATES

RATI SALUJA[1,*], K. M. MOEED[2]

[1]Department of Mechanical Engineering,
Goel Institute of Technology and Management, Lucknow, India
[2]University Polytechnic, Integral University, Lucknow, India
*Corresponding Author: ratisaluja@gmail.com

Abstract

An experimental investigation to study the influence of welding current, arc voltage and shielding gas flow rate on micro-hardness distribution of Grade 304L steel using pulse gas metal arc welding (pulse-GMAW) was accomplished. In this research, three factors, five levels full factorial central composite rotatable design has been practised to craft mathematical model and to associate micro-hardness distribution of 304L weld with pulse gas metal arc welding process variables. Efforts have also been made to correlate the influence of the cooling rate and alloying elements on micro-hardness of Grade 304L welded steel plates. The results indicate process parameters have profound effects in alteration of the micro-hardness distribution of weld. It was observed that at low cooling rates, micro-hardness of the weld was least and increases as the cooling rate was increased. Investigations have also reported that cooling rate and alloying elements significantly vary micro-hardness, Chromium equivalent to Nickel equivalent (Cr_{eq}/Ni_{eq} ratio), and ferrite content for Grade 304L steels weld samples. Weld-solidification results in Ferritic-Austenitic (FA) mode that was found extremely receptive to both process parameters and weld-composition.

Keywords: Austenitic stainless steel, Central composite rotatable design, Ferrite, Micro-hardness distribution, Pulse-gas metal arc welding.

1. Introduction

The Austenitic Stainless Steels (ASSs) have wide prospects of application in industries due to its high-quality corrosion and oxidation resistance in addition to superior mechanical properties [1]. These steels are subjected to sensitization, when implemented at high temperatures, either in manufacturing or in service [2]. Mechanical properties of Grade 304L ASSs are dependent on the relative change in microstructure as well as micro-texture [3]. Modification in mechanical properties is a consequence of segregation of alloying elements. Non-homogenous distribution of alloying elements settles a compositional fluctuation, between parent metal, Heat Affected Zone (HAZ) and weld-zone, concluding with variation in mechanical and metallurgical properties [4]. Dissimilarity in properties crops up due to the formation of intermetallic compounds and precipitation of metallic carbides [5]. Coring, which the influence of cooling rate on phase transformation ($F \rightleftharpoons A$) in the welded zone of steel is also an essential feature [6].

Moslemi et al. [7] had studied the influence of current on microstructure and mechanical performances on 316 steel. They concluded that optimum properties were attained under moderate current for Gas Metal Arc Welding (GMAW) process using ER-316 L as filler wire. Silva et al. [8] had accounted for the presence of carbon-rich austenite phases in API X80 steel pipe through various heat treatments. Their research emphasised on combined effects of carbon content and microphase's formation (ferrite and martensite) in weld microstructure. They reported a boost in micro-hardness was attributable to the occurrence of martensite islands and increased grain size of both the ferrite phase and martensite islands in the microstructure. Koga et al. [9] had lessened the consequences of cooling rate on solidification mechanisms and micro-hardness, on various types of boron-containing austenitic steels. Their research concluded that hardness of steel significantly varies with variation in carbon content and cooling rate. Unnikrishnan et al. [10] had analysed the effect of heat input variation on the microstructure of 304 L steel Shielded Metal Arc (SMA) welds. They reported an increase in secondary dendritic arm spacing with an increase in cooling rate. Kotecki [11] had explored the effect of process parameters on ASSs using flux cored arc welding. A mathematical model was developed between process parameters and deposited nitrogen content.

Gas Metal Arc Welding (GMAW) is one of the most cost-effective, trustworthy, multi-process modes of operations and widely adapted technique for fabrication of ASSs due to its easy application, high control over process variables, high productivity, and spatter-free quality weldments [12]. Pulse-GMAW has been preferred for joining of stainless steel as in spite of several advantages, stainless steel is prone to angular-distortion, hot-cracking, the formation of delta ferrite and sigma phase embrittlement, etc. [13]. Although several researches have been conducted to analyse the effect of heat input and cooling rate on mechanical performances of steels, regardless of, there have been little investigations on the interaction and quadratic effects of process parameters on the micro-hardness of 304 L pulse GMA welds and their association to root causes. Especially, the effect of compositional elements on micro-hardness of Grade 304L steel is rarely investigated. In most of the researches, implementation of the design matrix was not exercised [14-19].

To keep accuracy in prediction, control and optimisation, for prediction of weld-geometry, mechanical and metallurgical properties, it is mandatory to implement levels of input variables according to levels of the design matrix. Hence, to analyse analytical solution for determination of micro-hardness, three factors, five levels full factorial central composite rotatable design has been practised with Analysis of Variance (ANOVA)

technique for the development of the mathematical model. Central Composite Rotatable Design (CCRD) is preferred to minimise the number of trial runs in experiments, thus, saving cost and time. The overall principles of current research are sequenced below:

- Determination of micro-hardness distribution for weld-zone, heat affected zone and base metal with Vicker's hardness tester along with the development of the mathematical model for micro-hardness of Grade 304L weld and effect of process parameters on weld-profile.
- Correlation of micro-hardness with chemical composition of the welded region, ferrite number and phase transformation concerning cooling rate.

2. Experimental Procedure

In the current research, the pulse-GMAW is opted for conduction of experiments. The experiments were performed using ESAB Aristo MIG/MAG U5000I advance multi-process synergic pulse welding machine. This is a three-phase, 50 Hz, 500 A, 100% duty cycle welding machine along with integrated Weldcloud 2.0 version software. A commercially used Grade 304L ASSs was selected as a base metal. Samples of required dimensions (in mm) (300×150×6) were prepared from 6 mm thick hot-rolled steel plate according to American Society for Testing and Materials (ASTM) E3-11 standards. American Welding Society (AWS) A 5.9 ER-308 LSi filler wire of 1.2 mm diameter is used as filler metal. The chemical compositions of the parent and filler metal are mentioned in Table 1.

Table 1. Chemical compositions of grade 304 L ASSs and ER 308 LSi.

Type	*C* %	*Mn* %	*S* %	*Cr* %	*Ni* %	*P* %	*Si* %	*N* %	*Cu* %	*Mo* %
Parent metal	0.03	2.0	0.03	18.0-20.0	8.0-12.0	0.045	0.75	0.10	-	-
Filler wire	0.03	1.0-2.5	0.03	19.5-22.0	9.0-11.0	0.03	0.65-1.0	0.060	0.75	0.75

3. Assessment of process parameters

3.1. Identification of process parameters

To examine the micro-hardness changes during weld-solidification, amendment in heat input and cooling rate is essential [20]. Hence, welding current (*I*) and arc voltage (*U)* are opted as independent process variables [21].

Welding speed is also one of the significant variables, but when *I* and *U* are selected as independent process variables, the welding speed has to be altered to fill the filler metal in weld-joint. Therefore, welding speed is not selected as an independent variable in the present investigation. To study the considerable influence of cooling rate, shielding gas flow rate (*Q*) is varied to quench the solidification face. The experimental conditions and process variables opted for the fabrication of joints are displayed in Tables 2 and 3.

Table 2. Experimental conditions and process variables.

Variable	Shielding gas	Groove	Joint-type	Weld area	Root gap
Value	*Ar* 98% + O_2 2%	V groove with 60°	Butt	42 mm^2 approximately	2 mm
Variable	**Oscillation**	**Electrode stick out**	**Welding technique**	**Welding speed**	**Number of layers**
Value	No (string bead)	15 mm	Left-side	12 mm/s	Double pass

3.2. Fixing the limits of the process variables

The operational ranges of the entire elected variables were measured through trial runs. Trial runs were conducted by fixing all the variables with respect to one variable, whose range was quantified. Minimal five levels of input variables imitate the true conduct of output variables in CCRD as mentioned in Table 3. Therefore, the upper and lower limit ($\pm\alpha$) of given factors were coded as + 1.682 and -1.682 respectively [α = (number of factorial runs) $^{1/4} = (2^k)^{1/4} = (2^3)^{1/4}$, thus, $\alpha = 1.682$]. The intermediary values (-1, 0, +1) were computed with Eq. (1) [22, 23].

$$X_i = 1.682\left[\frac{2X-(X_{max}+X_{min})}{(X_{max}-X_{min})}\right] \quad (1)$$

Table 3. Welding parameters with their units, notation and levels.

Process parameters	Units	Notation	Levels				
			-1.682	**-1**	**0**	**1**	**1.682**
Voltage	Volt	*U*	25	26	27	28	29
Shielding gas flow rate	Liters/min	*Q*	10	12	14	16	18
Welding current	Amperage	*I*	220	226	235	244	250

4. Development of Design Matrix

Implementing the Design of Experiments (DOE) in a welding process makes it easier to link response (micro-hardness-distribution) with metallurgical properties (change in chemical composition, Cr_{eq}/Ni_{eq}, ferrite content, solidification phases), due to variation in independent input variables. The design matrix with three-factor five level CCRD with full replication technique for selected process variables is implemented. Design matrix displayed in Table 4 comprise with eight factorial runs (2^3 = 8, 2 is number of levels), six centre runs (0, 0, 0) and six star runs {(±1.682,0,0), (0,±1.682, 0), (0,0,±1.682)}. Random runs were channelized to evade errors during the investigational procedure [24]. Thus, total of 20 investigational points of central composite rotatable design permit evaluation of the linear, quadratic and two way interactive effects of the process parameters on the micro-hardness distribution of Grade 304L steel.

5. Recording the Responses

5.1. Determination of micro-hardness distribution on weld zone, heat affected zone and base metal with Vicker's hardness tester

The samples for microstructural examination and micro-hardness were acquired from the thickness section (vertical to the direction of the flow of welded-section) of 304 L ASSs plate. Micro-hardness of the Weld Zone (WZ), Heat Affected Zone (HAZ) and Base Metal (BM) was measured using a BIE make model BV-250 Vicker's micro-hardness tester using a load of 1 kg with a step range of 0.5 mm.

Measurements were carried out at six data points to obtain the value of micro-hardness on WZ, HAZ and PM. Accordingly, an average value of micro-hardness was documented. The observed micro-hardness for all three zones is given in Table 4. Predicted values of micro-hardness for weldments are tabulated in Table 5. It has been observed from results that for similar process parameters micro-hardness

diverged to some extent for investigational runs (15-20) due to the presence of noise-factor. It has also been analysed that the highest HAZ-hardness was found beneath the weld-bead in close proximity to the fusion zone.

Table 4. Coded design matrix with observed and predicted micro-hardness for weld, HAZ and parent metal.

S. No	Run order	Coded parameters			Cooling rate (*R*)	Weld zone	HAZ	Parent metal
		I (*A*)	*U* (*V*)	*Q* (*L/min*)		Observed micro-hardness	Observed micro-hardnes	Observed micro-hardness (h_{po})
1	2	-1	-1	-1	12.194	196	197	161
2	10	1	-1	-1	11.294	179	189	159
3	13	-1	1	-1	11.323	190	193	160
4	9	1	1	-1	10.488	186	194	159
5	15	-1	-1	1	12.194	212	202	162
6	3	1	-1	1	11.294	184	194	160
7	16	-1	1	1	11.323	193	193	161
8	18	1	1	1	10.488	178	192	160
9	7	-1.682	0	0	12.063	203	199	162
10	19	1.682	0	0	10.615	176	191	159
11	12	0	-1.682	0	12.196	193	198	160
12	11	0	1.682	0	10.514	185	195	160
13	17	0	0	-1.682	11.293	186	189	160
14	4	0	0	1.682	11.293	191	194	160
15	20	0	0	0	11.293	187	187	162
16	6	0	0	0	11.293	186	187	159
17	14	0	0	0	11.293	187	188	160
18	1	0	0	0	11.293	187	188	160
19	8	0	0	0	11.293	187	187	159
20	5	0	0	0	11.293	187	186	160

Table 5. Observed and predicted micro-hardness, residuals, SSE and standard deviation (σ), 3σ for welded samples.

S. No.	Run order	Welded region					
		Observed micro-hardness (H_{wo}) *HV*	Predicted Micro-hardness (H_{wp}) *HV*	Residuals (e_u)	*SSE*	*SD*(σ)	3σ
1	2	196	195.72	0.1866	0.0348	0.0174	0.0522
2	10	179	178.70	0.1866	0.0348	0.0174	0.0522
3	13	190	190.23	0.2631	0.0692	0.0346	0.1038
4	9	186	186.21	0.1866	0.0348	0.0174	0.0522
5	15	212	211.29	-0.8551	0.7312	0.3656	1.0968
6	3	184	183.27	0.7059	0.4983	0.2492	0.7475
7	16	193	192.81	-0.3760	0.1414	0.0707	0.2120
8	18	178	177.79	-0.3225	0.1040	0.0520	0.1560
9	7	203	203.32	0.1866	0.0348	0.0174	0.0522
10	19	176	176.38	-0.2345	0.0550	0.0275	0.0825
11	12	193	193.96	0.1866	0.0348	0.0174	0.0522
12	11	185	184.74	0.3030	0.0918	0.0459	0.1377
13	17	186	185.84	-0.9616	0.9247	0.4623	1.3870
14	4	191	191.86	0.2134	0.0455	0.0228	0.0683
15	20	187	186.81	-0.2120	0.0449	0.0225	0.0674
16	6	186	186.81	0.1909	0.0364	0.0182	0.0547
17	14	187	186.81	-0.8134	0.6616	0.3308	0.9924
18	1	187	186.81	0.1566	0.0245	0.0123	0.0368
19	8	187	186.81	0.2805	0.0787	0.0393	0.1180
20	5	187	186.81	0.7284	0.5306	0.2653	0.7959

In general, enhancement in micro-hardness is a tribute to the formation of fine grains in WZ and coarse grain refinement in HAZ due to variation in a thermal gradient. These changes can be attributed to thermal cycles produced during intermittent heating/cooling of the weld, fusion zone and HAZ [25]. As the highest heat is soaked by this portion, which results in solid-state transformation of F→A (austenitic grain growth), ultimately results in hardness enhancement of weld [26]. The micro-hardness of HAZ and WM is found more than BM. It can be associated with an increase in heat input that enhances the stress and grain coarsening, consequently increases Primary Dendrite Arm Spacing (PADS) and Secondary Dendrite Arm Spacing (SDAS) between dendritic grains and arms respectively [27, 28]. These transitions directly influence micro-hardness of Grade 304L steel, hence weld hardness increases.

Additionally, investigations reveal that an increase in current and voltage (cooling rate is inversely proportional to both process variables) reduces the micro-hardness of the weld. The possible reason is the formation of fine grains due to lesser heat acquired by WZ. According to Morris [29], "Hall Petch behaviour" lesser is the grain size, larger is the micro-hardness. Thus, the formation of fine grains increases the micro-hardness at higher cooling rates (12.063 ^{o}C/s - 12.194 ^{o}C/s). Micro-hardness of HAZ is also found greater than BM micro-hardness for all welded specimens. This behaviour is attributable to recrystallization of coarse grains into fine grains in HAZ. This behaviour continues for all intermediate values of cooling rate (≈11.294 ^{o}C/s). For an equal amount of cooling endowed (12.194 ^{o}C/s) for weld-specimen 1, 5 and 11, variation in weld microhardness was noticed from 193 HV to 212 HV as displayed in Figs. 1(a), (e) and (k). This kind of modification in micro-hardness was subjected to alteration of shielding gas flow rate. As the increase in shielding gas flow rate considerably increases the effect of cooling rate, consequently increases the micro-hardness of the weld.

Similar trends of micro-hardness variations were not found for HAZ (197-202 HVN). At low cooling rates (10.488 ^{o}C/s to 10.514 ^{o}C/s), low values of micro-hardness have been discerned for steel samples 4, 8, 10 and 12 as demonstrated Figs. 1(d) and (h) and Figs. 2(j) and (l). This phenomenon can be understood with "inverse Hall Petch" behaviour in which, micro-hardness reduces due to the occurrence of the coarser grain of bigger grain size [29]. In weld-samples, 5 and 9 micro-hardness of the weld (212 HV and 203 HV) is monitored more than micro-hardness of HAZ (202 HV and 199 HV) as shown in Figs. 1(e) and (i). This increase in hardness can be correlated with excess carbide precipitation and increased carbon content (0.0250 and 0.0254 wt %) in comparison to other weld samples. Figures 1(a), (c) and (g) and Figs. 2(o) to (t) of weld-samples 1, 3, 7 and 15-20, illustrate that values of micro-hardness of weld were found approximately equal to micro-hardness of HAZ.

This similarity could be accolade with minimal level (0 or -1) of welding current used. It also concludes that variation in micro-hardness of HAZ and WM can be maintained for approximately equal values for the lower magnitude of welding current. Differentiating the weld macrograph, the noticeable influence of process parameters was experienced for conducted investigation. Weld volume was found directly proportional to the amount of welding current and voltage used. The excessive root penetration with wider HAZ has been obtained for weld-samples 4, 8 and 10 as displayed in Figs. 1(d), 1(h) and Fig. 2(j). Moderate cooling rate (10.488 ^{o}C/s and 10.615 ^{o}C/s) and high heat input were found as the root cause of excessive root penetration. In Figs. 1(c), (d), (g), (h) and Fig. 2(l), increased weld-width has been noticed for the high value of arc voltage for weld samples 3, 4, 7, 8 and 12.

Due to the application of argon (shielding gas) and double pass welding Lack of Penetration (LOP) was not obtained. For an approximately equal amount of cooling endowed (12.194 ºC/s) for weld-specimen 1, 5 and 11, variation in weld microhardness was noticed from 193 HV to 212 HV for weld samples 1, 3, 5, 7, 9 and 11 as demonstrated in Figs. 1(a), (c), (e), (g), (i) and Fig. 2(k).

Modification in micro-hardness was seen due to alteration in shielding gas flow rate. A similar trend of higher variation was not found for microhardness of HAZ (197-202 HV).

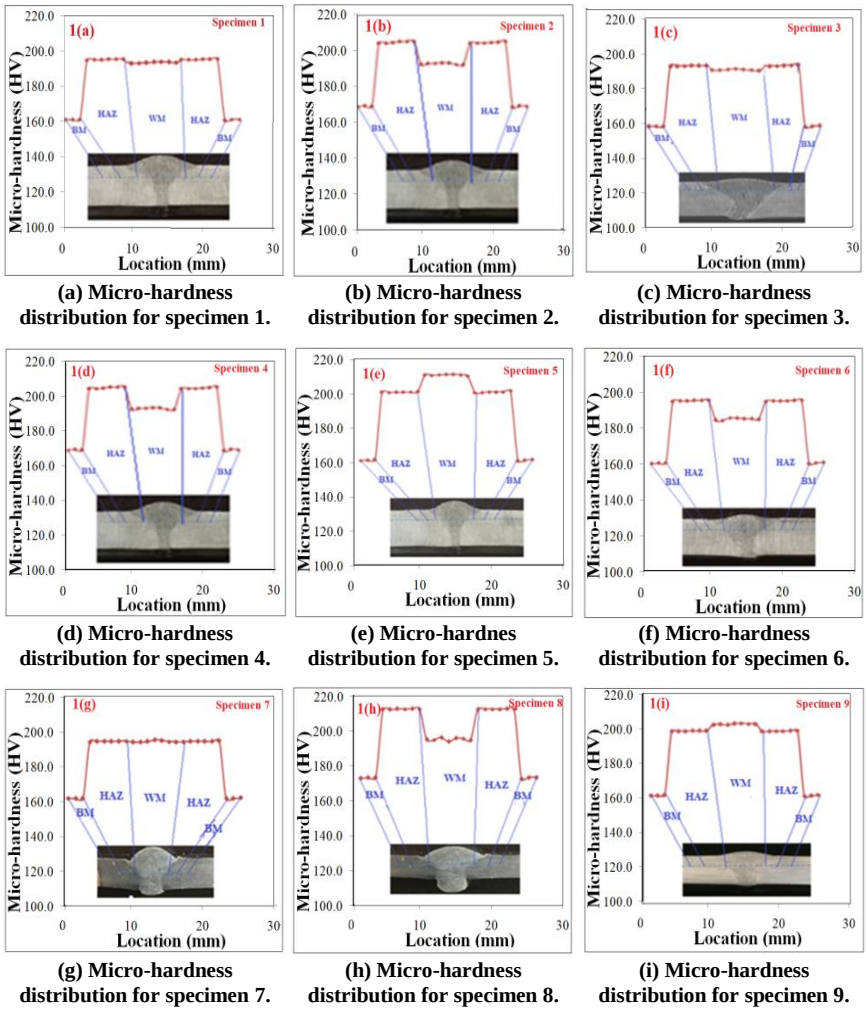

(a) Micro-hardness distribution for specimen 1. **(b) Micro-hardness distribution for specimen 2.** **(c) Micro-hardness distribution for specimen 3.**

(d) Micro-hardness distribution for specimen 4. **(e) Micro-hardnes distribution for specimen 5.** **(f) Micro-hardness distribution for specimen 6.**

(g) Micro-hardness distribution for specimen 7. **(h) Micro-hardness distribution for specimen 8.** **(i) Micro-hardness distribution for specimen 9.**

Fig. 1. Micro-hardness distribution with weld-macrograph according to design matrix for specimen 1 to 9.

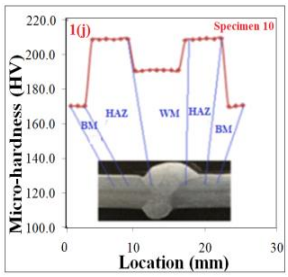

(j) Micro-hardness distribution for specimen 10.

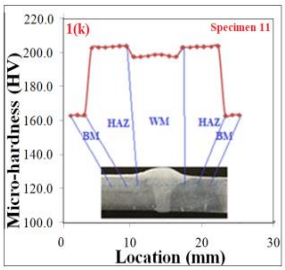

(k) Micro-hardness distribution for specimen 11.

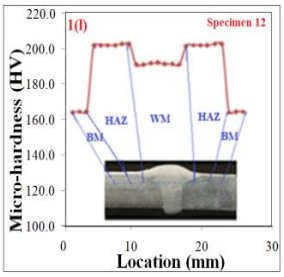

(l) Micro-hardness distribution for specimen 12.

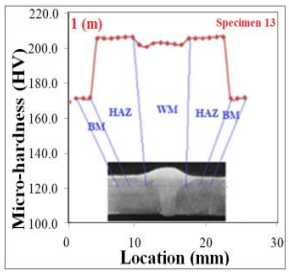

(m) Micro-hardness distribution for specimen 13.

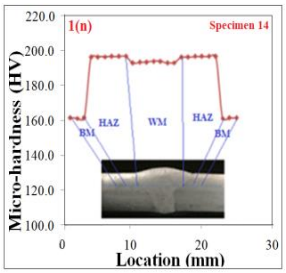

(n) Micro-hardness distribution for specimen 14.

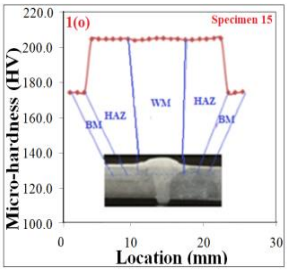

(o) Micro-hardness distribution for specimen 15.

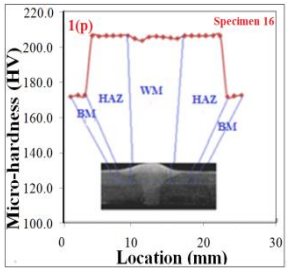

(p) Micro-hardness distribution for specimen 16.

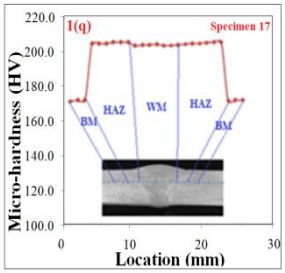

(q) Micro-hardness distribution for specimen 17.

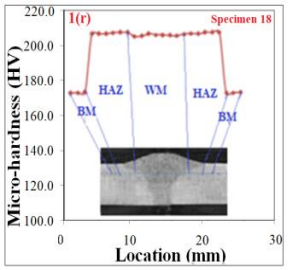

(r) Micro-hardness distribution for specimen 18.

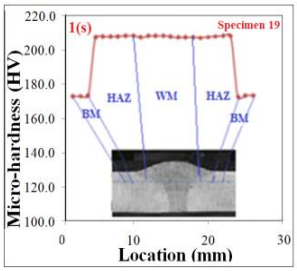

(s) Micro-hardness distribution for specimen 19.

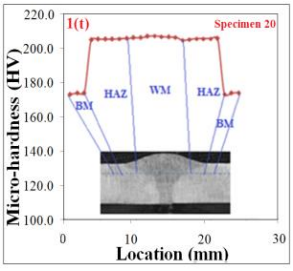

(t) Micro-hardness distribution for specimen 20.

Fig. 2. Micro-hardness distribution with weld-macrograph according to design matrix for specimen 10 to 20.

5.2. Correlation among micro-hardness of welded regions and phase transformation

The several theories state that ferrite number is a function of welding process variables, as well as of chemical composition of the weld-deposits [30]. Literature states that the Cr_{eq}/Ni_{eq} ratio within 1.48-1.95 (FA-mode) is preferable to achieve primary ferrite and secondary austenite in Grade 304L SS as well as for susceptibility to hot cracking in ASSs weld [31, 32].

The compositional constituent that forms solid-solution in ferrite also influence its micro-hardness. The micro-hardness can be increased or else decreased with pragmatic development of substitutional solution with the distinction of alloying elements. Hence, the interaction between micro-hardness, ferrite number, Cr_{eq}/Ni_{eq} and alloying elements had been lessened for Grade 304 steel specimens. Carbon, nickel, chromium, silicon, manganese and nitrogen binary and ternary alloys are selected to investigate the primary cause of variation in micro-hardness and FN.

Ferrite number had been computed with ferrite scope Fischer FMP30. The wet analysis was exercised for estimation of carbon weight percent for all welded-samples and remaining compositional investigation was quantified with spectrographic tests. Empirical relations of WRC-1992 nickel and chromium equivalency were used to predict Cr_{eq}, $Ni_{eq,}$ for 304 L welded specimens [32, 33].

Chemical compositions of these p-GMAW welded ASSs specimens are given in Table 6. The measured Cr_{eq}/Ni_{eq} ratio was found in between 1.39 to 1.67 that signifies the FA mode of solidification for all Grade 304L ASSs welded specimens.

Ferrite content between 4.8 FN to 8.0 FN also reassured that weld metal had fallen into FA-mode [34]. It is inferred that the micro-hardness of weld-zone increases with the increase of cooling rate, it can be associated with increased martensite content in the weld. At a higher cooling rate, micro-hardness of WM increases due to delayed ferrite-development. As excess retained ferrite promotes the formation of pearlite and martensite in weld structure. The micro-hardness of martensite enhances rapidly with the addition of carbon in the weld.

In addition, the micro-hardness also increases with increase in alloying elements content such as nickel, chromium, molybdenum, silicon and manganese. Nitrogen had a profound however negative influence on the micro-hardness of weld-zone.

It has been noticed from Table 6 that carbon, silicon and manganese play a relatively strong contributory role on the micro-hardness of the weld and at the same time as chromium influences the least. Influence of nitrogen was also found appreciable, whether the impact of nickel was sensed, intermediary. Molybdenum had instituted lesser impact on micro-hardness still influence was more effective than chromium.

Table 6. Alloying composition, Cr_{eq}/Ni_{eq} and ferrite number for welded-specimens.

S. No.	*C*	*Cr*	*Ni*	*Mo*	*Si*	*Mn*	N_2	Cr_{eq}/Ni_{eq}	Ferrite number (FN)
1	0.0248	21.76	11.15	0.516	0.69	1.31	0.115	1.56	7.9
2	0.0246	20.65	10.45	0.436	0.64	1.21	0.145	1.48	6.2
3	0.0248	21.40	10.63	0.485	0.67	1.32	0.127	1.56	6.8
4	0.0246	20.10	10.13	0.460	0.66	1.17	0.167	1.44	4.8
5	0.0254	21.82	11.98	0.571	0.73	1.40	0.085	1.54	7.3
6	0.0247	20.71	10.29	0.432	0.66	1.17	0.152	1.49	5.6
7	0.0249	21.65	11.04	0.534	0.68	1.33	0.109	1.57	7.5
8	0.0245	20.32	10.03	0.445	0.65	1.20	0.160	1.47	5.4
9	0.0250	21.80	11.44	0.564	0.71	1.35	0.099	1.56	8.0
10	0.0243	20.13	10.64	0.423	0.64	1.15	0.165	1.39	4.9
11	0.0249	20.74	10.47	0.424	0.68	1.34	0.125	1.53	6.7
12	0.0247	20.71	10.70	0.427	0.67	1.19	0.121	1.51	5.7
13	0.0245	20.80	10.02	0.459	0.66	1.32	0.134	1.57	6.8
14	0.0249	21.85	11.01	0.511	0.68	1.33	0.131	1.54	6.9
15	0.0247	20.83	10.44	0.475	0.67	1.26	0.124	1.55	6.8
16	0.0246	20.46	10.45	0.467	0.67	1.26	0.122	1.52	6.8
17	0.0247	20.65	10.57	0.486	0.66	1.25	0.124	1.52	6.8
18	0.0247	20.63	10.58	0.463	0.67	1.24	0.125	1.51	6.8
19	0.0247	20.51	10.71	0.458	0.68	1.25	0.129	1.48	6.7
20	0.0247	20.82	10.48	0.427	0.68	1.26	0.127	1.53	6.8

6. Mathematical model

The micro-hardness of the weld can be represented as a function of response as $H_w = f(I, U, Q)$. The response surface methodology based on second order regression technique was implemented to structure the mathematical model and for prediction of micro-hardness of welded samples as expressed in Eq. (2).

$$Y = b_o + \sum_{i=1}^{k} b_i X_i + \sum_{i=1}^{k} b_{ii} X_i^2 + \sum_{i=1}^{k} b_{ij} X_i X_j + \varepsilon_i \quad (2)$$

Here b_0 symbolizes free term of the response regression equation, the coefficients b_i signify linear terms, the coefficients b_{ii} stand for quadratic terms, the coefficients b_{ij} are interaction terms and term represents ε_i is an error in model [35].

The final mathematical model in terms of coded variables was built with the help of regression coefficients given in Table 7. For statistical analysis and development of a mathematical model, design-expert 11.0 software was used [36].

Regression coefficients with less significance were removed and the final regression equation is crafted for prediction of micro-hardness of weld in Vickers Hardness scale (HV).

$$H_w = 186.813 - 8.011(I) - 2.743(U) + 1.787(Q) + 1.073(I^2) - 0.899(U^2) + 0.72(Q^2) + 3.25(I\,U) - 2.75(I\,Q) - 3.25(UQ) + \varepsilon \quad (3)$$

The predicted weld micro-hardness (H_{wp}), residual (e_u), residuals Sum Of Square Terms *(SSE)*, standard deviation (σ) and 3σ evaluated as displayed in Table 5.

Variance imitates Lack of Fit (*LOF*) of the regression model from observed responses. Computation of standard error *(ε)* is not viable as it varies with each observation, hence, the use of residuals (e_u) analyse discrepancy between observed and predicted response values in experimental design.

7. Validation of Coefficients for Significance

Regression coefficients indicate control of the process-parameters on response. Positive regression coefficient indicates a positive alliance between process parameters whether a negative value of regression coefficient indicates the inverse relationship between variable and response [37].

The *F* and *p*-values, with the sum of squares and mean squares are mentioned in Table 7. The model *F*-value of 338.29 implies the model is significant. There is only a 0.05% chance that an *F*-value this large could occur due to noise. *P*-values less than 0.05 indicate model terms are significant.

In this case, *I, U, Q, IU, IQ, UQ, I², U², Q²* are significant model terms. Values greater than 0.05 indicate the model terms are not significant.

The Lack of Fit (*LOF*)'s *F*-value of 4.05 implies that there is a 7.53% chance that *F*-value this large could occur due to noise hence insignificant.

Table 7. Test of significance for regression coefficients.

Source	Coefficient estimate	Sum of squares (SS)	*DF*	Mean square (MS)*	*F*-value*	*P*-value*	Significance *(p<0.05)*
Model	-	1282.34	9	142.48	338.29	0.0001	Significant
I	186.81	876.50	1	876.50	2081.03	0.0001	Significant
U	-8.01	102.72	1	102.72	243.88	0.0001	Significant
Q	-2.74	43.63	1	43.63	103.58	0.0001	Significant
IU	1.79	84.50	1	84.50	200.63	0.0001	Significant
IQ	3.25	60.50	1	60.50	143.64	0.0001	Significant
UQ	-2.75	84.50	1	84.50	200.63	0.0001	Significant
I²	-3.25	16.60	1	16.60	39.42	0.0001	Significant
U²	1.07	11.58	1	11.58	27.50	0.0004	Significant
Q²	0.8966	7.47	1	7.47	17.73	0.0018	Significant
Residual	-	4.21	10	0.4212	-	-	-
Lack of fit (LOF)	-	3.38	5	0.6757	4.05	0.0753	Not Significant
Error	-	0.8333	5	0.1667	-	-	-
Total	-	1286.55	19	-	-	-	-

*MS = SS/DF, F-value = MS of LOF/ Ms of error terms, R-value = (MS of 1st order term and 2nd order term)/MS of error term

8. Validation of Results

Fit statics of response is given in Table 8. The adjusted regression model is weighed against a full regression model with (R^2). The predicted coefficient of determination (R^2) of 0.9792 is in reasonable agreement with the adjusted coefficient of determination of 0.9938; i.e., the discrepancy is less than 0.2. 'adequate precision' quantifies the signal-to-noise ratio (*S/N* ratio). Computed *S/N* ratio equals to 76.09, which signifies a satisfactory signal as a minimum four of *S/N* ratio is enviable.

Table 8. Fit statistics of micro-hardness (weld).

Coefficient of determination (R^2)			Standard error ($1-R^2$)			Adequate Precision = (*S/N* ratio
Full model	**Adjusted model**	**Predicted model**	**Full model**	**Adjusted model**	**Predicted model**	
0.9967	0.9938	0.9792	0.0033	0.0062	0.0208	76.0905

9. Results and Discussion

The developed regression equation was applied for prediction of micro-hardness of the welded region (H_w) by placing the relevant values of the selected input variables (I, V, Q). A developed mathematical model is exercised to analyse direct and interaction influence of input variables over micro-hardness of the weld.

9.1. Direct effect of welding current on micro-hardness

From the Fig. 3, it can be inferred that micro-hardness decreases with increase in arc current from 220 A to 250 A. Increase in welding current increases heat input, which in turn reduces the cooling rate. Reduction in cooling rate increases the solidification time that promotes the formation of coarser dendrites and results with a reduction in micro-hardness [11, 38]. This phenomenon can be simply understood with "Hall Petch" equation expressed in Eq. (4).

$$H = H_o + K_H d^{-1/2} \tag{4}$$

Here H is micro-hardness of steel as a function of grain diameter d, H_o and K_H are constants. According to the Hall-Petch equation, micro-hardness is the reciprocal root of the grain size. Thus, smaller the grain size is, higher is the micro-hardness [39]. Hence, an improvement is found in micro-hardness of the weld as the magnitude of welding current is increased.

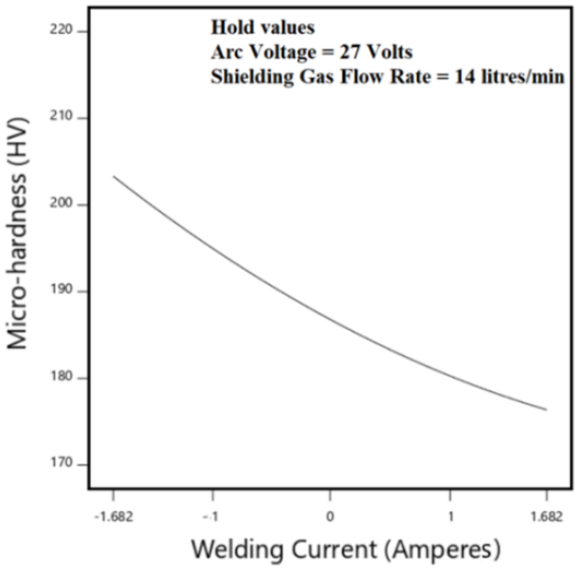

Fig. 3. Effect of welding current on micro-hardness (weld).

9.2. Direct effect of arc voltage on micro-hardness

Figure 4 shows the effect of arc voltage on micro-hardness. From the figure, it can be inferred that hardness decreases, as the arc voltage is increased from 25 V to 29 V. It can also be interpreted as, at a low value of voltage, heat input ($E = f(U)$) decreases.

The reduction in heat input results with a drop in temperature difference, thus, increases the cooling rate. Increased cooling rate promotes the formation of finer dendrites, as less solidification time is available [10]. Hence, micro-hardness increases due to the formation of fine dendrites in the welded zone [38].

9.3. Direct effect of shielding gas flow rate on micro-hardness

Figure 5 shows the effect of shielding gas flow rate on micro-hardness. From the figure, it is clear that micro-hardness increases as the shielding gas flow rate is increased from 10 to 18 L/min. This is due to the fact that the shielding gas carries away heat during welding.

This reduces the span of solidification time and enhances the cooling rate. A rapid cooling cycle with a large undercooling will increase the number of nuclei and reduces the size of resulting dendrites. It often leads to the formation of small grains that ultimately results in increased micro-hardness of weld [11, 29].

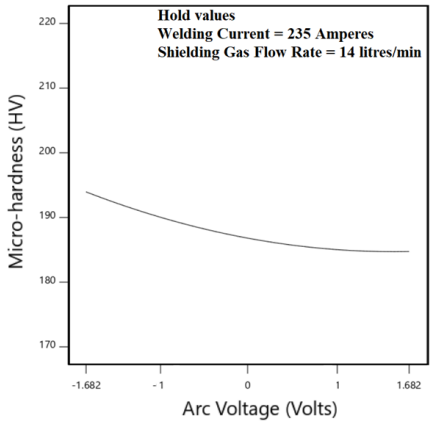

Fig. 4. Effect of arc voltage on micro-hardness (weld).

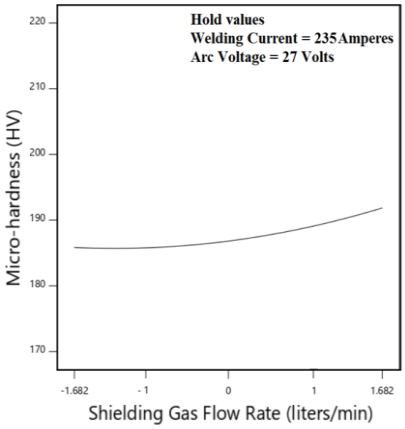

Fig. 5. Effect of gas flow rate on micro-hardness (weld).

9.4. Interactive effects between arc voltage and welding current on micro-hardness

Figure 6(a) shows the interactive effect of arc voltage and welding current on micro-hardness. Shielding gas flow rate for analysing interactive effects between arc voltage and welding current is set to 14 L/min (centre value of DOE). It has been inferred from the direct effect analysis that both welding current and arc voltage has a negative effect on the micro-hardness of the weld. Micro-hardness variation is noticed for arc voltage at 25 V to 29 V, if welding current is increased from 220 A to 250 A. Micro-hardness decreases to 2.81 % when arc voltage increases from 26 to 27 volts and further decreases 2.70% when voltage reaches 29 V (maximum star value for voltage) for a fixed current value 220 A. The percentage of decrease of micro-hardness is found 4.89% when arc voltage increases from 25 V to 29 V to for a fixed current 226 A. It falls to 2.04% for same arc voltage when current is increased to 230A. The value of micro-hardness found 186 HV to 190 HV for intermediate values of arc voltage (27 V) and current (235 A). Drastic fall in micro-hardness had been obtained, when the current value is increased beyond 240 A.

Thus, it can be inferred that the increase is higher at lower welding current and voltage and low at higher current and voltage. This is attributable to the heat input given *(E =f (I, U)).* Increase in the magnitude of current and voltage, increase the heat input. This, in turn, reduces the cooling rate. Consequently, more solidification time is available for dendritic growth, thus, micro-hardness of weld reduces with increase in grain-size [29, 39].

From the response surface plot shown in Fig. 6(b), it is clearly inferred that micro-hardness of weld reaches a minimum of 174 HV when the welding current is at 250 A and the arc voltage is at 29 V. Micro-hardness reaches a maximum of 219 HV when the welding current is at 220 A and arc voltage is at 25 V. The percentage increase in micro-hardness is very high at low welding currents, but gradually declines as the welding current is increased. This trend changes for voltage value at 28 V. These effects are elucidated through a contour plot displayed in Fig. 6(b).

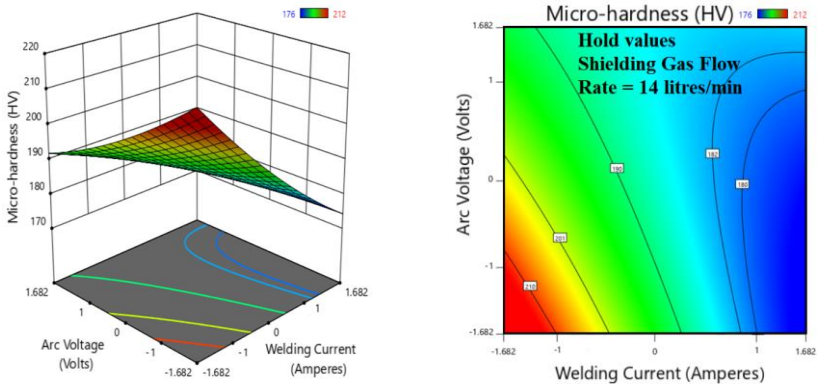

(a) Response surface plot showing interactive effects between welding current and arc voltage for micro-hardness (weld).

(b) Contour plot displaying interaction effects of welding current and arc voltage for micro-hardness (weld).

Fig. 6. Interactive effects of welding current and arc voltage for micro-hardness (weld).

9.5. Interactive effects of welding current and shielding gas flow rate on micro-hardness

It is previously conferred from the direct analysis that micro-hardness of weld decreases as arc current is increased from 220 A to 250 A and increases as the shielding gas flow rate is increased from 10 to 18 L/min. The interaction effects of welding current and shielding gas flow rate on weld micro-hardness is explained with the help of the response surface and contour plot given in Figs. 7(a) and (b). Response surface plot displays that maximal value of micro-hardness (215 HV) is obtained for the minimum value of welding current at 220 A and maximum value of shielding gas flow rate at 18 L/min. The percentage decrease for micro-hardness is 4.87 % for the same value of welding current (220 A) when the shielding gas flow rate is reduced to 18 L/min.

When welding current is increased to 226 A. Micro-hardness reduction percentage increases to 6.02% for a similar variation of shielding gas flow rate from 10 L/min to 18 L/min. For the intermediate value of welding current at 235 A, minor variation in micro-hardness (186 HV to 190 HV) is observed when the gas flow rate is varied from its minimal axial to maximal axial value.

Micro-hardness further increases to 182 HV when welding current is increased from 240 A to 250 A for an approximate value of shielding gas flow rate at 10 L/min. Micro-hardness of 180 HV is obtained for welding current at 250 A when shielding gas flow rate is kept at 12 L/min. Variation in micro-hardness can associate with the mutual effect of both the process parameters. Whether at one hand the increase in shielding gas flow carries away heat during welding, on the other side increase in heat input is obtained with an increase in welding current. This mutual effect of both parameters varies the cooling rate. A rapid cooling rate reduces the size of resulting dendrites that consequently increases the micro-hardness [29, 39]. Thus, it can be assessed with a fixed value of welding current, modification in micro-hardness can be attained by varying the shielding gas flow rate to an extent.

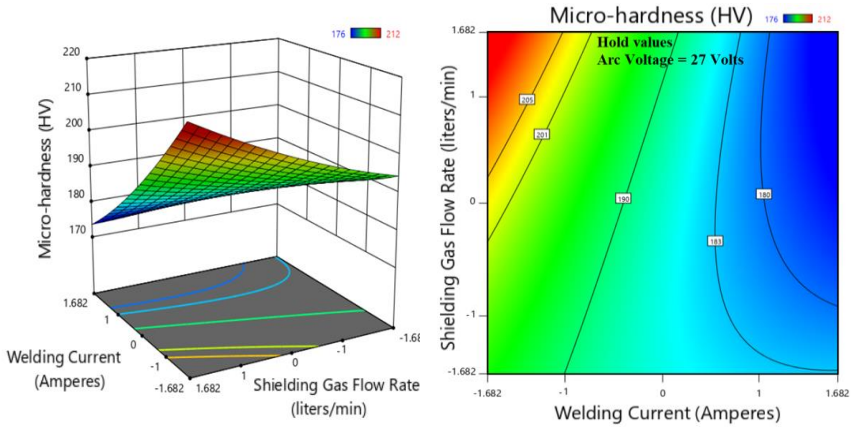

(a) Response surface plot showing interactive effects between welding current and gas flow rate for micro-hardness (weld).

(b) Contour plot displaying interaction effects of welding current and gas flow rate for micro-hardness (weld).

Fig. 7. Interactive effects of welding current and shielding gas flow rate for micro-hardness (weld).

9.6. Interactive effects of arc voltage and shielding gas flow rate on micro-hardness

It has been inferred from the direct effect analysis that arc voltage has a negative effect on micro-hardness and shielding gas has a positive effect on micro-hardness. The interaction effects of voltage and shielding gas flow rate on weld micro-hardness are demonstrated with the help of the response surface and contour plot given in Figs. 8(a) and (b). From the response surface plot, it can be noticed that maximum hardness (208 HV) is achieved at minimum arc voltage 25 V and shielding gas flow rate 18 L/min. For voltage at 25 V and the value of shielding gas flow rate at 13 L/min, micro-hardness was found 190 HV. When the shielding gas flow rate was increased to 16

L/min, an increase of 2.81% is noticed in micro-hardness of the weld. On further increasing the gas flow rate for the same voltage micro-hardness increased by 1% approximately. At 27 V when shielding gas flow rate is varied from 10 L/min to 18 L/min, micro-hardness was found in the range of 186-190 HV. It is observed that the micro-hardness decreases for arc voltage at 28 V and further increases for 29 V as the shielding gas flow rate was increased. The percentage of decrease for hardness was 1.88% for arc voltage at 28 V when the shielding gas flow rate varies from 10 L/min to 16 L/min. A similar trend was observed for arc voltage at 29 V for shielding gas flow rate 12 L/min to 15 L/min. Minimal micro-hardness (178 HV) was obtained at a maximum arc voltage 29 V and shielding gas flow rate 18 L/min. Alteration in micro-hardness value is because of interaction effects of gas flow rate and arc voltage. This effect is as similar as discussed for welding current and shielding gas flow rate. The shielding gas provides an additional cooling at the time of welding, whether arc voltage enhances the heat input [10, 23]. The mutual outcome of both variables alters the cooling rate, ultimately variation in micro-hardness is obtained due to variation in cooling rate. Thus, micro-hardness of weld varies with variation in arc voltage and shielding gas flow rate.

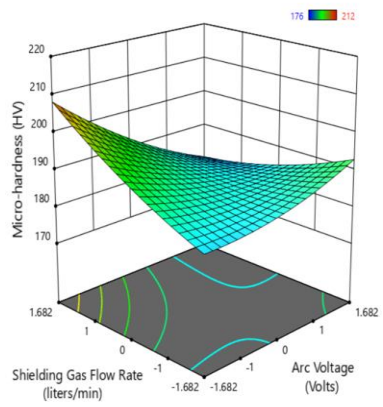

(a) Response surface plot showing interactive effects between arc voltage and gas flow rate for micro-hardness (weld).

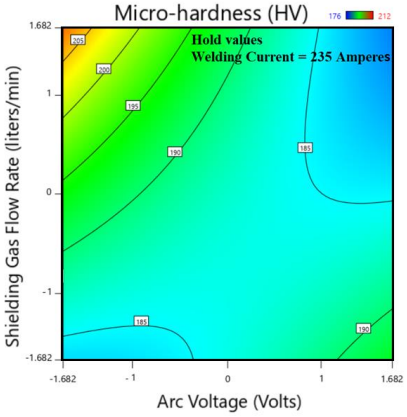

(b) Contour plot displaying effects of arc voltage and gas flow rate for micro-hardness (weld).

Fig. 8. Interaction effects of shielding gas flow rate and arc voltage on micro-hardness (weld).

10. Conclusions

The experiments had been conducted for prediction of micro-hardness distribution on 304 L austenitic stainless steel. The efforts had been made to understand the influence of process and metallurgical parameters on micro-hardness of welded plates. A number of concluding interpretations from the experimental analysis are given below.

- The second-order quadratic mathematical model is developed using full factorial central composite design with process variables (welding current, arc voltage and shielding gas flow rate) for prediction of micro-hardness for Grade 304L ASSs. The predicted results were compared with experimental

results for a 5% level of significance. The standard error *(1- R^2)* of the predicted model (0.0208) is found minimum than standard error of full model (0.0033) and adjusted model (0.0062). Therefore, validation of results indicates that the calculated mathematical model can be implemented for prediction of response (micro-hardness of weld) in design space.

- The coded equation was found very useful for identifying the relative impact of the factors by comparing the factor's coefficients. It is also concluded that shielding gas flow rate has a positive influence on micro-hardness, whether the influence of welding current and arc voltage was found negative. The effect of welding current was found more influencing rather than the other two parameters.
- The minimum micro-hardness of weld attained was 176 HV, for welding current at 226 A, arc voltage at 26 V and shielding gas flow rate at 16 L/min. Maximum micro-hardness of the weld was 215 HV for welding current at 220 A, arc voltage at 26 V and shielding gas flow rate at 18 L/min. The micro-hardness of the weld is found in permissible range of accepted hardness for 304 L welds, hence it can be concluded that according to the preference of micro-hardness range, process parameters can be selected.
- The micro-hardness of base metal is found lesser in comparison to the hardness of HAZ and WM as an increase in heat input enhances the stress and grain coarsening. Micro-hardness is found increased with increase in ferrite content in the 304 L weld. It was also verified that cooling rate highly affects micro-hardness of 304 L welds.
- Cr_{eq}/Ni_{eq} ratio revealed the presence of FA solidification mode in the weld. Ferrite number measurement (4.8 FN to 8.0 FN) with ferrite meter also affirms the presence of FA mode.
- Influence of alloying elements over micro-hardness is also investigated and revealed that micro-hardness also increases with increase in selected alloying elements as carbon, nickel, chromium, molybdenum, silicon and manganese. Effect of nitrogen was found negative on the micro-hardness of weld-zone.

Nomenclatures

A_w	Weldment area, mm^2
b_i	Linear term
b_{ii}	Quadratic term
b_{ij}	Interactive term
b_o	Free term of regression equation
d	Grain diameter, μm
E	Heat input, J
H	Hardness of steel, $(H_o + K_H d^{-1/2})$
H_o	Constant in Eq. (4)
H_w	Hardness of weld, HV
I	Welding current, A
K_H	Constant in Eq. (4)
Q	Gas flow rate, L/min
R	Cooling rate, $^oC/s$
S	Welding speed, mm/s

t_c	Critical-time in cooling, s
U	Arc voltage, volts
X	Process variable
X_i	Coded value of process variable
X_{max}	Upper limit of process variable
X_{min}	Lower limit of process variable

Greek Symbols

γ	Austenite phase
δ	Ferrite phase

Abbreviations

ANOVA	Analysis of Variance
ASSs	Austenitic Stainless Steel
BM	Base Metal
CCRD	Central Composite Rotatable Design
Cr_{eq}/Ni_{eq}	Chromium Equivalent to Nickel Equivalent
FA	Ferritic-Austenitic
FN	Ferrite Number
GMAW	Gas Metal Arc Welding
HAZ	Heat Affected Zone
PGMAW	Pulse Gas Metal Arc Welding
RSM	Response Surface Methodology
SMAW	Shielded Metal Arc Welding
WZ	Weld-Zone

References

1. Sencer, B.H.; Was G.S.; Sagisaka M.; Isobe Y.; Bond G.M.; and Garner, F.A. (2003). Proton irradiation emulation of PWR neutron damage microstructures in solution annealed 304 and cold-worked 316 stainless steels. *Journal of Nuclear Materials*, 323(1), 18-28.
2. Ma, J.C.; Yang, Y.S.; Tong, W.H.; Fang, Y.; Yu, Y.; and Hu, Z.Q. (2007). Microstructural evolution in grade, 304 stainless steel during directional solidification and subsequent solid-state transformation. *Materials Science and Engineering: A*, 444(1-2), 64-68.
3. Saha, S.; Mukherjee, M.; and Pal, T.K. (2015). Microstructure, texture, and mechanical property analysis of gas metal arc welded AISI 304 austenitic stainless steel. *Journal of Materials Engineering and Performance*, 24(3) 1125-1139.
4. Yan, J.; Gao, M.; and Zeng, X. (2010). Study on microstructure and mechanical properties of 304 stainless steel joints by TIG, laser and laser-TIG hybrid welding. *Optics and Lasers in Engineering*, 48(4), 512-517.
5. Shen, Y.F.; Li, X.X.; Sun, X.; Wang, Y.D.; and Zuo, L. (2012). Twinning and martensite in a 304 austenitic stainless steel. *Materials Science and Engineering: A*, 552, 514-22.
6. Fu, J.W.; Yang, Y.S.; Guo, J.J.; and Tong, W.H. (2008). Effect of cooling rate on solidification microstructures in AISI 304 stainless steel. *Materials Science and Technology*, 24(8), 941-944s.

7. Moslemi, N.; Redzuan, N.; Ahmad, N.; and Hor, T.N. (2015). Effect of current on characteristic for 316 stainless steel welded joint including microstructure and mechanical properties. *Procedia CIRP*, 26, 560-564.
8. Silva, R.d.A.; de-Souza, L.F.G.; Morales, E.V.; Rios, P.R.; and Bott, I.d.S. (2015). Formation of microphases and constituents from remaining austenite decomposition in API X80 steel under different processing conditions. *Materials Research*, 18(5), 908-917.
9. Koga, G.Y.; Otani, L.B.; Silva, A.M.B.; Roche, V.; Nogueira, R.P.; Jorge Jr., A.M.; Bolfarini, C.; Kiminami, C.S.; and Botta, W.J. (2018). Characterization and corrosion resistance of boron-containing-austenitic stainless steels produced by rapid solidification techniques. *Materials*, 11(11), 2189.
10. Unnikrishnan, R.; Idury, K.S.N.S.; Ismail, T.P.; Bhadauria, A.; Shekhawat, S.K.; Khatirkar, R.K.; and Sapate, S.G. (2014). Effect of heat input on the microstructure, residual stresses and corrosion resistance of 304L austenitic stainless steel weldments. *Materials Characterization*, 93, 10-23.
11. Kotecki, D.J. (1978). Welding parameters effects on open arc stainless steel weld metal ferrite. *Welding Journal (AWS)*, 76(1), 109s-117s.
12. Gholipour, A.; Shamanian, M.; and Ashrafizadeh, F. (2011). Microstructure and wear behavior of satellite 6 cladding on 17-4 PH stainless steel. *Journal of Alloys and Compounds*, 509(14), 4905-4909.
13. Mukherjee, M.; and Pal, T.K. (2012). Influence of mode of metal transfer on microstructure and mechanical properties of gas metal arc-welded modified ferritic stainless steel. *Metallurgical and Materials Transactions A*, 43(6), 1791-1808.
14. Chao, J.; and González-Carrasco, J.L. (1998). Influence of cooling rate on room temperature tensile behaviour of thermally oxidised MA 956. *Materials Science and Technology*, 14(5), 440-444.
15. Perdrix, F.; Trichet, M.-F.; Bonnentien, J.-L.; Cornet, M.; and Bigot, J. (2001). Influence of nitrogen on the microstructure and mechanical properties of Ti-48Al alloy. *Intermetallics*, 9(2), 147-155.
16. Serre, I.; and Vogt, J.-B. (2008). Heat treatment effect of T91 martensitic steel on liquid metal embrittlement. *Journal of Nuclear Materials*, 376(3), 330-335.
17. Baek, J.-H.; Kim, Y.-P.; Kim, W.-S.; and Kho, Y.-T. (2001). Fracture toughness and fatigue crack growth properties of the base metal and weld metal of a type 304 stainless steel pipeline for LNG transmission. *International Journal of Pressure Vessels and Piping*, 78(5), 351-357.
18. Zumelzu, E.; Sepulveda, J.; and Ibarra, M. (1999). Influence of microstructure on the mechanical behaviour of welded 316L SS joints. *Journal of Materials Processing Technology*, 94(1), 36-40.
19. Wang, J.; Xiong, J.; Peng, Q.; Fan, H.; Wan, Y.; Li, G.; and Shen, B. (2009). Effects of DC plasma nitriding parameters on microstructure and properties of 304L stainless steel. *Materials Characterization*, 60(3), 197-203.
20. Smith, W.F. (1993). *Structure and properties of engineering alloys* (2nd ed.). New York, United States of America: McGraw-Hill Science.
21. Ghosh, P.K. (2017). Concept of pulse current gas metal arc welding proces. *Pulse Current Gas Metal Arc Welding*, 31-45.

22. Murugan, V.V.; and Gunaraj, V. (2005). Effect of process parameters on angular distortion of gas metal arc welded structural steel plates. *Welding Journal (AWS)*, 84(11), 165s-171s.
23. Sudhakaran, R.; Murugan, V.V.; Sivasakthivel, P.S.; Balaji, M. (2013). Modeling and analysis of ferrite number of stainless steel gas tungsten arc welded plates using response surface methodology. *The International Journal of Advanced Manufacturing Technology*, 64(9-12), 1487-1504.
24. Cochran, W.G.; and Cox, G.M. (1992). *Experimental designs* (2nd ed.). Hoboken, New Jersey, United States of America: John Wiley & Sons, Inc.
25. Ha, X.H.; Jang, S.W.; Bang, W.H.; Yoon, U.-S.; and Oh, K.H. (2002). Texture evolution in weld regions of SUS-304 stainless steel and TRIP steel. *Material Science Forum*, 408-412, 1377-1382.
26. Arata, Y.; Matsuda, F.; and Katayama, S. (1976). Fundamental investigation on solidification behaviour of fully austenitic and duplex structures and effect of ferrite on microsegregation. *Transactions of JWRI*, 5(2), 35-51.
27. Kasuya, T.; and Hashiba, Y. (2007). Carbon equivalent to assess hardenability of steel and prediction of HAZ hardness distribution. *Nippon Steel Technical Report No. 95*, 53-61.
28. EL-Bealy, M.; and Thomas, B.G. (1996). Prediction of dendrite arm spacing for low alloy steel casting processes. *Metallurgical and Materials Transactions B: Process Metallurgy and Materials Processing*, 27(4), 689-693.
29. Morris, J.W. (2001). The influence of grain size on the mechanical properties of steel. *Technical Report No. LBNL-47875*. Lawrence Berkeley National Laboratory, Berkeley, California, United States of America.
30. Padilha, A.F.; Tavares, C.F.; Martorano, M.A. (2013). Delta ferrite formation in austenitic stainless steel castings. *Materials Science Forum*, 730-732, 733-38.
31. Kotecki, D.J.; and Siewert, T.A. (1992). WRC-1992 Constitution diagram for stainless steel weld metals: A modification of the WRC- 1988 diagram. *Welding Journal* (AWS), 71, 171s-178s.
32. Saluja, R.; and Moeed, K.M. (2012). The emphasis of phase transformations and alloying constituents on hot cracking susceptibility of type 304L and 316L stainless steel welds. *International Journal of Engineering Science and Technology (IJEST)*, 4(5), 2206-2216.
33. McCowan, C.N.; Siewert, T.A.; Vigliotti, D.P.; and Wang, C.-M.J. (2001). Reference materials for weld metal ferrite content. *Welding Journal (AWS*), 80(4), 106s-114s.
34. Lippold, J.C.; and Kotecki, D.J. (2005). *Welding metallurgy and weldability of stainless steels* (1st ed.). Hoboken, New Jersey, United States of America: John Wiley & Sons, Inc.
35. Montgomery, D.C. (2003). *Design and analysis of experiments*. Hoboken, New Jersey, United States of America: John Wiley & Sons, Inc.
36. Stat Ease. (2019). Design-eExpert software version 12. Retrieved February 26, 2018 , from https://shop.statease.com/software/design-expert/.
37. Montgomery, D.C.; Peck, E.A.; and Vining, G.G. (2012). *Introduction to linear regression analysis (5th ed.).* Hoboken, New Jersey, United States of America: John Wiley & Sons, Inc.

38. Kumar, M.V.; Balasubramanian, V.; and Rao, A.G. (2015). Effect of filler addition on solidification behaviour and hot tensile properties of GTA-welded tube joints of Super 304H austenitic stainless steel. *International Journal of Mechanical and Materials Engineering*, 10(1), 25 pages.
39. Schino, A.D.; Barteri, M.; and Kenny, J.M. (2003). Grain size dependence of mechanical, corrosion and tribological properties of high nitrogen stainless steels. *Journal of Materials Science*, 38(15), 3257-3262.